Optical Engineering

SPIEDigitalLibrary.org/oe

Hyperspectral and high-resolution image fusion based on second generation Bandelet transform

Xiaoping Du
Hang Chen
Zhengjun Liu
Xiaojie Dou
Lurui Xia
Xiangzhen Cheng
Congmiao Shan

Hyperspectral and high-resolution image fusion based on second generation Bandelet transform

Xiaoping Du
Hang Chen
Academy of Equipment
Department of Space Command
Beijing 101416, China
E-mail: hitchenhang@foxmail.com

Zhengjun Liu
Harbin Institute of Technology
Department of Automation Measurement and Control
Harbin 150001, China

Xiaojie Dou
Lurui Xia
Xiangzhen Cheng
Congmiao Shan
Academy of Equipment
Department of Space Command
Beijing 101416, China

Abstract. A fusion algorithm of hyperspectral and high-resolution images based on principal component analysis (PCA) and second generation Bandelet transform is proposed. Primarily, the numerous components of the hyperspectral image are divided. Subsequently, the maximum rule is used to select the Bandelet coefficients and geometry flows of the hyperspectral image which are transformed by PCA in the following step. Finally, the fused image is reconstructed by taking inverse PCA and Bandelet transform. Some numerical simulations are made to test the validity and capability of the proposed fusion algorithm. © *2013 Society of Photo-Optical Instrumentation Engineers (SPIE)* [DOI: 10.1117/1.OE.52.6.067001]

Subject terms: hyperspectral; image fusion; Bandelet transform; multiscale.

Paper 130096 received Jan. 23, 2013; revised manuscript received Apr. 28, 2013; accepted for publication May 1, 2013; published online Jun. 3, 2013.

1 Introduction

The image processing of high spatial and high spectral resolutions is becoming the immediate area of research focus in remote-sensing applications. Image fusion of hyperspectral and high-resolution images has been proposed in order to make better use of these two kinds of images. Some fusion algorithms have been reported based on different methods such as principal component analysis (PCA), hue intensity saturation (HIS), wavelet transform, contourlet, and Bandelet transform.[1–6] As the mature algorithms, the PCA and HIS transformations have been researched extensively for color image fusion with red, green, and blue components.[1] These methods perform well in keeping spatial resolution. The spectral characteristics of the original images, however, will be distorted in varying degrees. Moreover, some fusion algorithms combined PCA or HIS with other methods have been employed for advancing image fusion algorithms.[7–9]

The wavelet transform and filter-bank method can preserve spectral information well, whereas some spatial resolutions of the panchromatic images are lost.[10] Recently, the developing algorithm based on contourlet transform has been employed in hyperspectral image fusion.[11] Besides, the latest multiscale transforms, like Bandelet and its second generation form, have also been used in image fusion.[12–14] These multiscale transforms perform well in multispectral image and panchromatic image. Experimental results of these algorithms show that the fused image by using multiscale transform performs more outstanding in keeping spatial detailed information and keeping global spectral information compared to those of the HIS method.[10–14]

In this paper, a novel hyperspectral image and high spatial resolution image fusion scheme by using PCA and second Bandelet transform is proposed. A specific band of the original hyperspectral image is divided into four sub-bands in every level until the sub-band is lower than the threshold we set before. To confirm the optimal direction of each tiny square, a sample method is introduced and applied.[15] Subsequently, Bandelet coefficients and geometries flows are calculated by using the second generation Bandelet transform.[4] Then, PCA transform is performed to calculate their principal component (PC) and they will be replaced by the high spatial resolution data in the following step. Numerical simulation is performed in order to validate the performance of the proposed image fusion algorithm.

The rest of the paper is organized in the following sequence. In Sec. 2, the experiment of capturing the original images and the proposed fusion algorithm is introduced in detail. In Sec. 3, numerical simulation results are made and given to demonstrate the validity of the algorithm. Concluding remarks are summarized in Sec. 4.

2 Capturing Images and the Fusion Algorithm

First, the experiment of capturing images is described in this section. Thereafter, the intact fusion algorithm based on the Bandelet transform is addressed in detail.

2.1 *Capturing Images*

Hyperspectral camera is of great importance in remote sensing due to its high spectral resolution. The original images in this paper are acquired by hyperspectral camera and a common high spatial resolution camera. The hyperspectral camera used in this research is Image-λ-V10E-PS, as shown in Fig. 1, and its basic parameters are listed in Table 1.

Fig. 1 The hyperspectral camera system.

In this experiment, the capture angle of the camera is controlled by the electric turntable, as shown in Fig. 1, and both the hyperspectral camera and high-resolution camera can be fixed on the turntable. In addition, to reduce the influence of ambient lighting changes, we captured the images at the same time. Here, infrared (IR) cut filter or polarizer are not used in the present experiment.

The digital images are multiplexed and transmitted to computer in real time. Subsequently, the data is submitted to the ancillary software for preprocessing, i.e., rayscale correction and denoising. The preprocessing is necessary because the systematic errors exist in this acquisition operation. Some recent methods can be performed to register the hyperspectral image and high spatial resolution image.[16,17] The registered images are illustrated in Fig. 2. The data in black frame is selected and calculated in this research.

Table 1 Basic parameter of the hyperspectral camera used in this research.

Spectrograph model	Image-λ-V10E-PS
Spectral range (nm)	400 to 1000
Spectral resolution (nm)	2.73
Numerical aperture	$F/2.4$
Slit size (μm)	30
Sensor pixel	1392×1040
Pixel size (μm)	6.45×6.45

2.2 *Second Generation Bandelet Transform*

The second generation Bandelet transform is a kind of orthogonal multiscale transform, proposed by Pennec and Mallat, on the base of Bandelet transformation in 2005.[4] The second generation Bandelet transform (hereafter referred to as Bandelet transform) is able to track the geometric regular direction of images and the characteristics of the image edges by selecting the best Bandelet basis adaptively. It notes that because of the nonboundary effect and the characteristic of global orthogonality, Bandelet basis is superior to the first generation Bandelet transform.[10]

The geometry flows and Bandelet coefficients of the original images are obtained by Bandelet transform. The image can be perfectly reconstructed by geometry flow and Bandelet coefficients due to the reversibility of Bandelet transform. The functions $G_j(i)$ and $C_j(i)$ represent the Bandelet coefficients and geometry flows in this paper, respectively. Here, i denotes the number of the specific band in a hyperspectral image. The average rule is chosen for geometric flow due to the fact that geometric flow is the description of the image edges, while maximum rule is chosen for Bandelet coefficients because they are gained in high sub-bands.[18] Next, the Bandelet transform will be explained in detail in the rest of this section.

2.2.1 *Quadtree segmentation*

First, the original image $f(x, y)$ is decomposed along the x and y directions by using two-dimensional (2-D) wavelet transform. The 2-D orthogonal wavelet decomposition function can be expressed as

$$\begin{cases} f_k(i,j) = \sum_m \sum_n f_{k-1}(x,y)\varphi(2x-i)\phi(2y-j) \\ f_k^H(i,j) = \sum_m \sum_n f_{k-1}(x,y)\varphi(2x-i)\phi(2y-j) \\ f_k^V(i,j) = \sum_m \sum_n f_{k-1}(x,y)\varphi(2x-i)\phi(2y-j) \\ f_k^D(i,j) = \sum_m \sum_n f_{k-1}(x,y)\varphi(2x-i)\phi(2y-j) \end{cases}, \quad (1)$$

where $f_k(i, j)$ is the low frequency information decomposed into No. k level. The symbol φ and ϕ denote the two-scale

(a) (b)

Fig. 2 The acquired images: (a) false color composite of the hyperspectral image and (b) high-resolution.

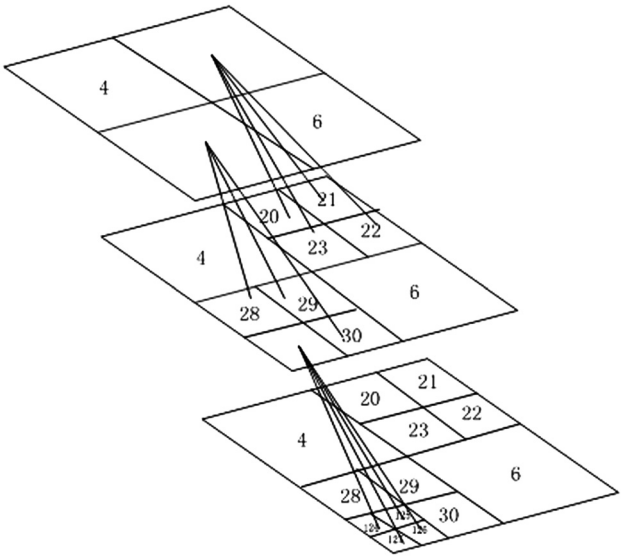

Fig. 3 The binary quadtree segmentation.

difference equation. The functions $f_k^H(i,j)$, $f_k^V(i,j)$, and $f_k^D(i,j)$ re related to the high frequency information of horizontal, vertical, and diagonal direction, respectively.

In order to perform the full algorithm presented in Ref. 4, quadtree segmentation[15] and geometric angle sampling are necessary to be introduced in this section. A binary quadtree segmentation process is performed as follows: one specific band of the hyperspectral image is divided into four sub-bands in every level until the sub-band is lower than the threshold.[19] The schematic of the quadtree segmentation is shown in Fig. 3.

2.2.2 *Geometric flow*

In Bandelet transform domain, the geometric flow of vector is defined to represent the edges of the image and it provides the general direction. To find the best direction in a tiny square, angle sampling is applied to select the optimal geometrical flow direction by

$$\theta = \frac{k\pi}{L^2-1}, k = 0, 1, 2, \ldots, L^2-2, \tag{2}$$

where L represents the size of square and θ means the circumferential angle of the square. As we can learn from Eq. (2), the circumferential angle in the range $[\theta, 2\pi]$ is divided into L^2-1 parts.

To compute the quadtree segmentation, we first calculate the Lagrange coefficients for each square in smallest size and then perform from the smallest size to largest size. After that, each group of four squares is merged and computed to figure out its Lagrangian. The Lagrange function can be expressed as

$$L(f,R) = \|f_\theta - \tilde{f}_\theta\| + \lambda T^2(R_g + R_b) \tag{3}$$

$$\tilde{f}_\theta(j,l,k) = \int_{R^2} f_\theta(x)\Phi_{j,l,k}(x)\mathrm{d}x, \tag{4}$$

where f_θ represents the true value of one-dimensional (1-D) wavelet coefficients of each subscale of image and $\tilde{f}_\theta$ represents the quantized coefficients of 1-D wavelet coefficients by using curvelet transform as shown in Eq. (4). The variable T denotes the quantization threshold. The parameters R_g and R_b represent the number of bit rate for geometric flow encoding and bit coefficients for Bandelet coefficients encoding, respectively. The symbols $\Phi_{j,l,k}(x)$ denotes the wavelet function, where j, l, and k denote the scale, direction, and displacement, respectively. The parameter λ denotes Lagrange factor. The quantization function is defined as

$$Q(x) = \begin{cases} 0, & \text{if } |x| \le T, \\ \mathrm{sgn}(x)(q+0.5), & \text{if } qT \le |x| \le (q+1) \end{cases}. \tag{5}$$

The Lagrange coefficients of every sampling angle are calculated by employing Eqs. (2) and (3). Figure out the minimum Lagrange coefficient, then, the corresponding sampling angle of the minimum Lagrange coefficient is the best geometric flow $G_j(i)$ we are looking forward. In addition, the Bandelet coefficients are computed in a high frequency sub-band by using the wavelet transform. The coefficients of wavelet are transformed by 1-D wavelet to generate the Bandelet coefficients $C_j(i)$ in each scale.

2.2.3 *PCA transform*

The PCA projects the higher correlation N-dimensional data to the orthogonal the M-dimensional subspace $(M \ll N)$.[20,21] Thus, the original data with large information can be represented as the new subspace with irrelevant and variance data.

PCs refer to the derived variables which are a linear combination of the original variables. Here, the geometric flows G_j in different scale of the hyperspectral image are arranged as a matrix as follows:

$$\begin{cases} Y_1 = u_{11}G_1 + u_{12}G_2 + \cdots + u_{1n}G_n \\ Y_2 = u_{21}G_1 + u_{22}G_2 + \cdots + u_{2n}G_n \\ \vdots \\ Y_n = u_{n1}G_1 + u_{n2}G_2 + \cdots + u_{nn}G_n \end{cases}, \tag{6}$$

where the eigenvector u are defined as

$$u_{k1}^2 + u_{k2}^2 + \cdots + u_{kn}^2 = 1, k = 1, 2, \ldots, n. \tag{7}$$

In Eq. (6), the quantity Y_1 has the maximum variance in all the linear combination of $G_1, G_2 \ldots G_n$. Similarly, Y_2 is irrelevant to Y_1 and has the largest variance in all the linear combination of $G_1, G_2 \ldots G_n$. Y_n is irrelevant to $Y_1, Y_2 \ldots Y_n$ and has the largest variance in all the linear combination of $G_1, G_2 \ldots G_n$. Here, Y_1 is the first PC variance and contains most information of the original data.

2.3 *Image Fusion Algorithm*

The flowchart of the fusion scheme is displayed in Fig. 4. To complete this fusion algorithm, PCA method is considered and utilized. First, the hyperspectral image is divided into every single band. The Bandelet transform is performed

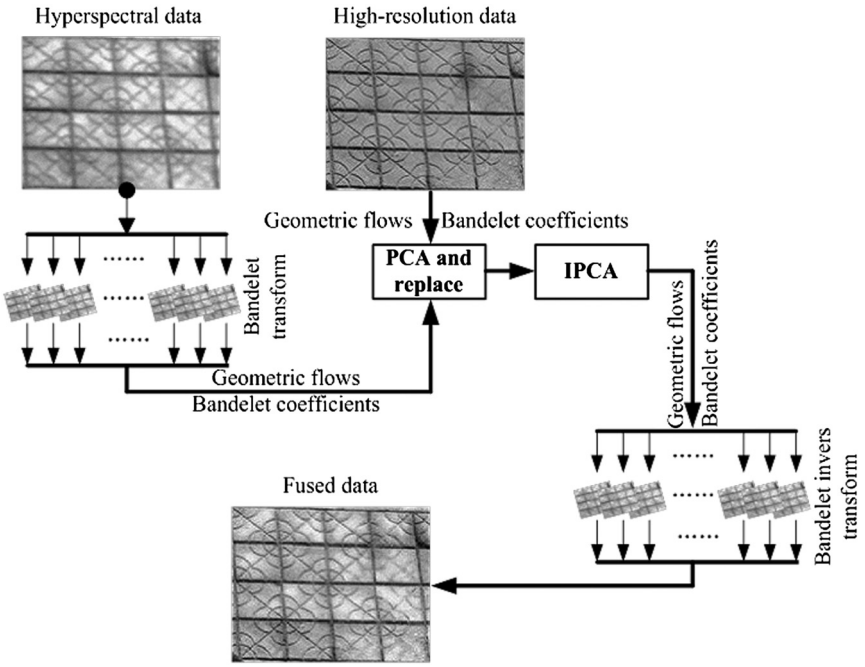

Fig. 4 The flowchart of the proposed fusion algorithm.

for each band of the image. For different scales, geometric flows, and Bandelet coefficients, which are calculated and converted into 1-D vectors, are transformed by PCA.

In the following step, the first PCs of the geometric flows are replaced by the high-resolution geometric flows due to the fact that the high-resolution geometric flows contain more high spatial details data. Here, the high-resolution geometric flows have a common structure of hyperspectral geometric flows since their scenes are no different. Both Bandelet transform and PCA are reversible. Consequently, the image reconstruction can be performed along the reverse direction of the front process with the inverse operations. In the Bandelet transform, the coefficients of hyperspectral and high-resolution image are mixed by the following equation:

$$C_j = \begin{cases} C_{\text{hyper}}, |C_{\text{hyper}}| \geq |C_{\text{high}}|, \\ C_{\text{high}}, |C_{\text{hyper}}| < |C_{\text{high}}|, \end{cases} \tag{8}$$

where C_{hyper} and C_{high} represent the Bandelet coefficients of hyperspectral image and high-resolution image, respectively.

3 Numerical Simulation

Numerical simulation, in this section, is considered for demonstrating of the fusion algorithm. A hyperspectral image and a high-resolution image having 256×256 pixels are regarded as the original images, which are shown in Fig. 5. The direction angle θ of each square satisfies uniform distribution in the range $[0, 2\pi]$. Objective performance evaluation criteria are employed in this paper, such as the standard deviation, average gradient, and mutual information. Moreover, subjective evaluation has also been described in detail in this section.

The hyperspectral image obtained from the experiment owns 520 bands from 400 to 1000 nm is selected merit-based. To simplify the calculation, the original data is

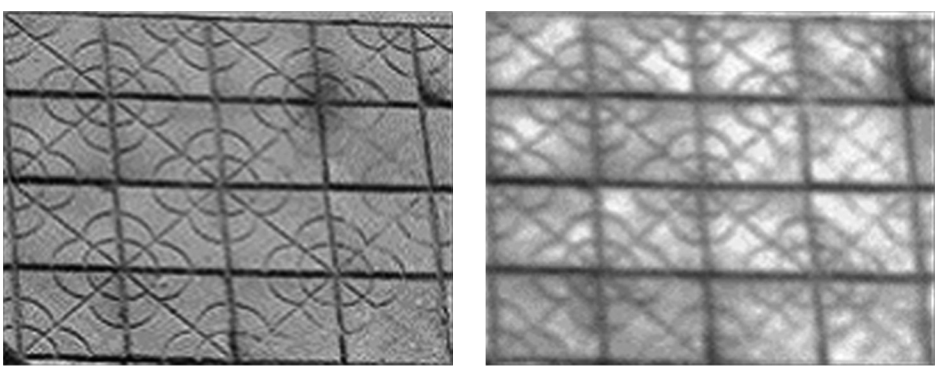

(a) (b)

Fig. 5 The acquired images: (a) high-resolution image and (b) specific band of the hyperspectral image.

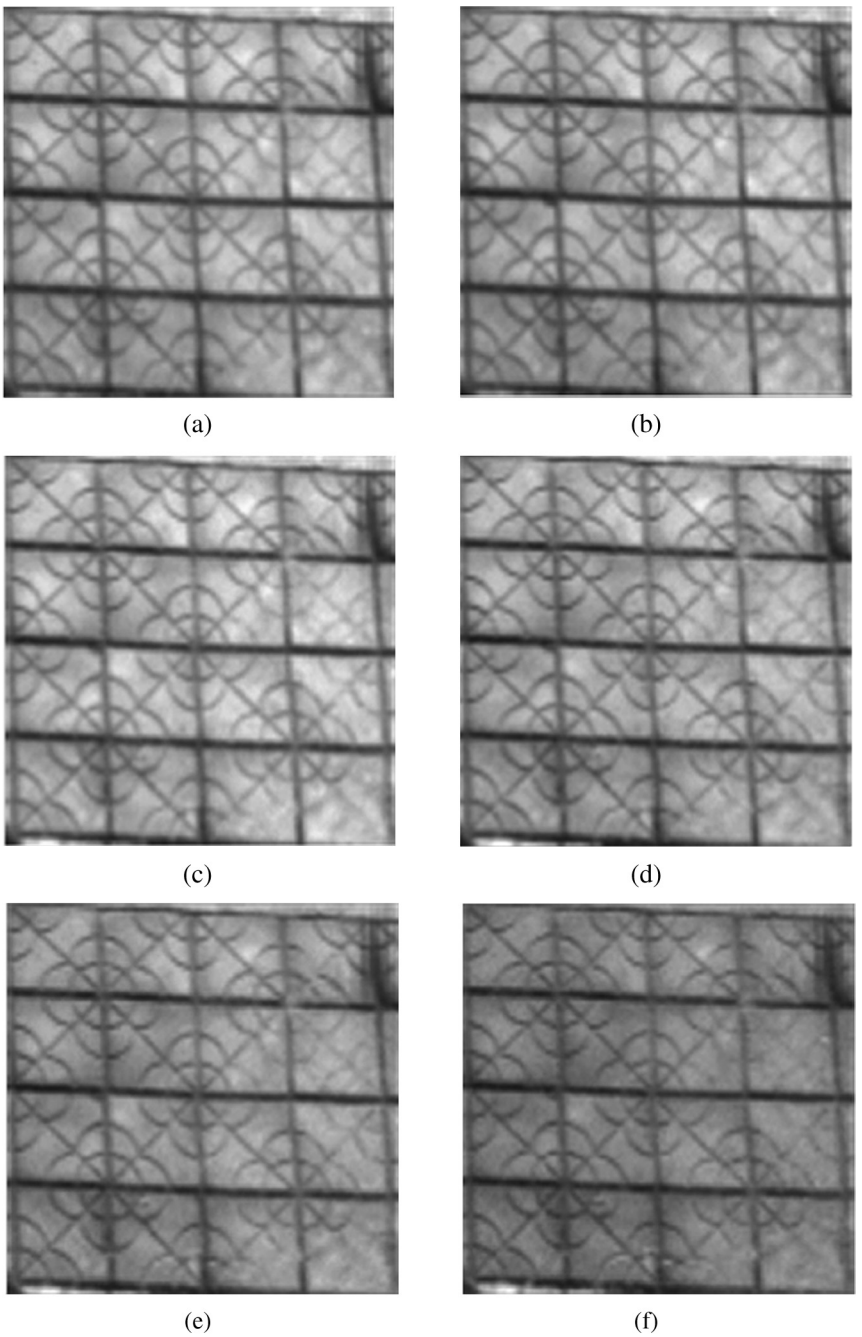

Fig. 6 The hyperspectral images: (a) 410 nm, (b) 590, (c) 610 nm, (d) 710 nm, (e) 810 nm, and (f) 910 nm.

equidistant sampled into 56 bands and eight of them are displayed in Fig. 6. The corresponding fusion images are shown in Fig. 7. From Figs. 6 and 7, the fused images are clearer than the hyperspectral image in visual observation. Meanwhile, the fused image contains more details and texture features than the original image by subjective assessment. Furthermore, standard deviation, entropy, and average gradient are applied to evaluate the fusion algorithm.[22] Larger standard deviation and entropy indicate that more information is contained in the fused images while the larger average gradient indicates richer detailed information. The statistics evaluation in detail is given in Table 2.

To weight the difference between the original images and the fusion images quantitatively, the relative mean square error (RMSE) function is introduced and defined as

$$\mathrm{RMSE} = \mathrm{rmse}(I_f, I_s) = \frac{\sum_{\forall m,n}[I_f(x,y) - I_s(x,y)]^2}{\max\left(\sum_{\forall m,n}[I_f(x,y)]^2, \sum_{\forall m,n}[I_s(x,y)]^2\right)}, \quad (9)$$

where I_f and I_s are the fused image and original standard image, respectively. The values of RMSE represent the difference of the two images. Now, we test the RMSE values

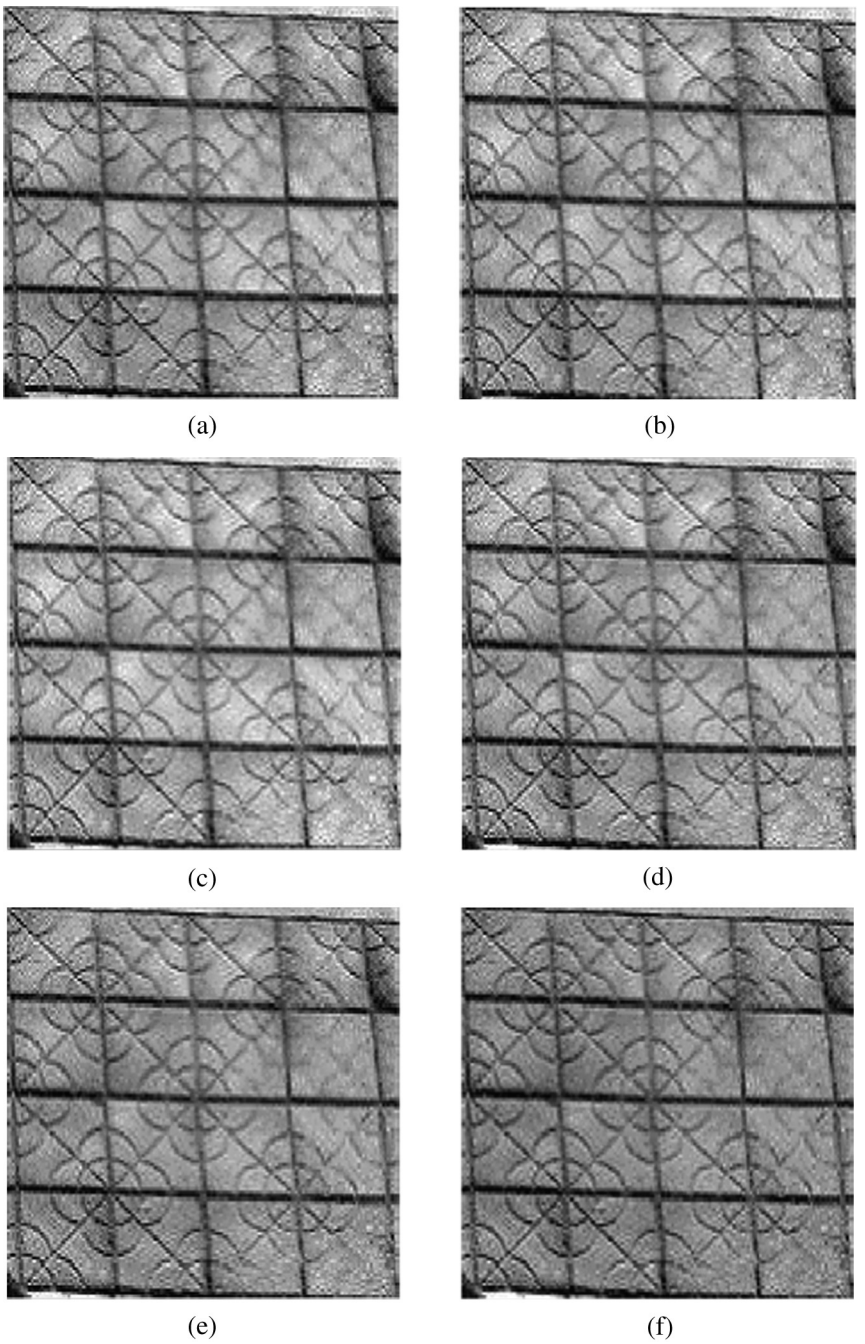

Fig. 7 The fused images: (a) 410 nm, (b) 590, (c) 610 nm, (d) 710 nm, (e) 810 nm, and (f) 910 nm.

Table 2 The statistics evaluation of hyperspectral images and fused images.

Images	Figure 6(a)	Figure 7(a)	Figure 6(c)	Figure 7(c)	Figure 6(e)	Figure 7(e)
Standard deviation	35.3436	45.9923	36.7379	46.4459	26.1147	41.6011
Average gradient	3.1170	9.6274	3.4933	9.5483	2.9079	9.5257
Entropy	6.8078	7.4148	7.1024	7.4173	6.6404	7.2254

between original image and hyperspectral image, original image and fused image, fused image and hyperspectral image, respectively. The RMSE curves are calculated and displayed in Fig. 8. The result has demonstrated that the fusion algorithm performs well in fusing information. The curve between fused images and hyperspectral images is steadier than the other two curves. In other words, the errors between fused images and hyperspectral images are steadier than the other two sets of data. In addition, the fusion algorithm is more prominent in the near-infrared band (780 to 1000 nm in this paper) from Fig. 8.

A single band of the multispectral image and a high-resolution panchromatic image, from IKONOS of Fuyang data, having 256×256 pixels are considered and utilized to test the proposed algorithm. The details of the venation in Fig. 9(a) cannot be identified entirely.

In this experiment, mature fusion methods of PCA, Laplacian pyramid, and ratio pyramid are used to compare with the performance of Bandelet fusion method proposed. The Laplacian pyramid and Filter Subtract Decimate pyramid are used with four of decomposition. The fused images from different algorithms are illustrated in Fig. 10.

Compared with the other fused images in Fig. 10, the fused image from the proposed fusion method is more distinct. More details and texture features can be seen in Fig. 10(d) than the other three fused images by subjective assessment. Besides, the edge information of Fig. 10(d) is more smooth and clear in the case of magnified observation due to the superior performance in tracking geometric regular and the characteristics of image edge by selecting best Bandelet basis.

The standard deviation, entropy, average gradient, and structural similarity index measurement system (SSIM) are also used to test the performance of fusion algorithms as mentioned above. The corresponding data are listed in Table 3. Figure 10(d) has larger standard deviation and entropy which means that more information appears in the fused images. The larger average gradient denotes richer detailed information. Values of RMSE between fused images and original high-resolution image in Table 3 show that the error of Fig. 10(d) is smaller than Fig. 10(a) and 10(b). In addition, a new indicator to measure the similarity of the two images, the SSIM, is shown in the last low of Table 3. The value between fused images and original high-resolution

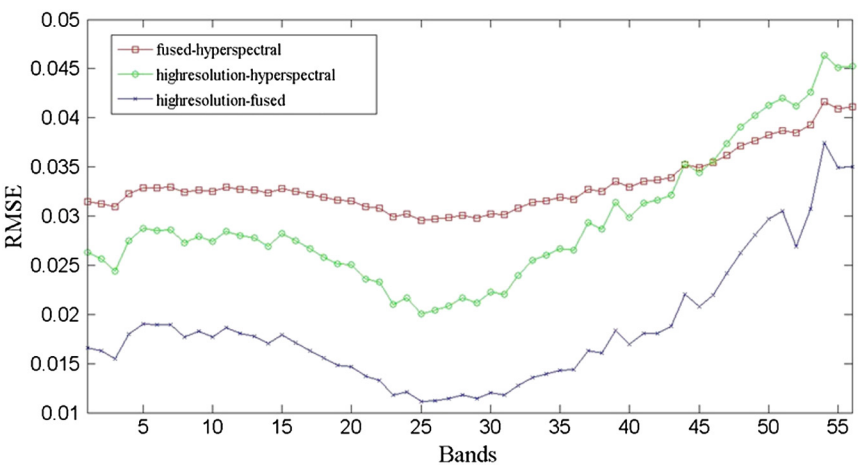

Fig. 8 The relative mean square error (RMSE) value between high-resolution, hyperspectral, and fused images.

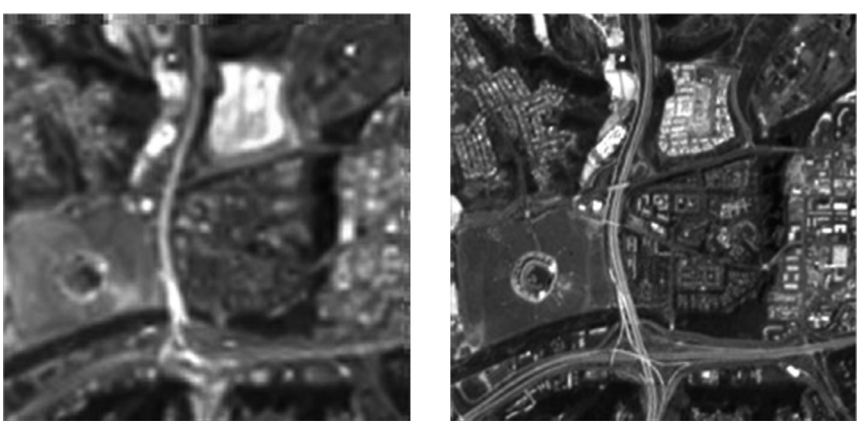

(a) (b)

Fig. 9 The experimental images: (a) specific band of the multispectral image and (b) high-resolution panchromatic image.

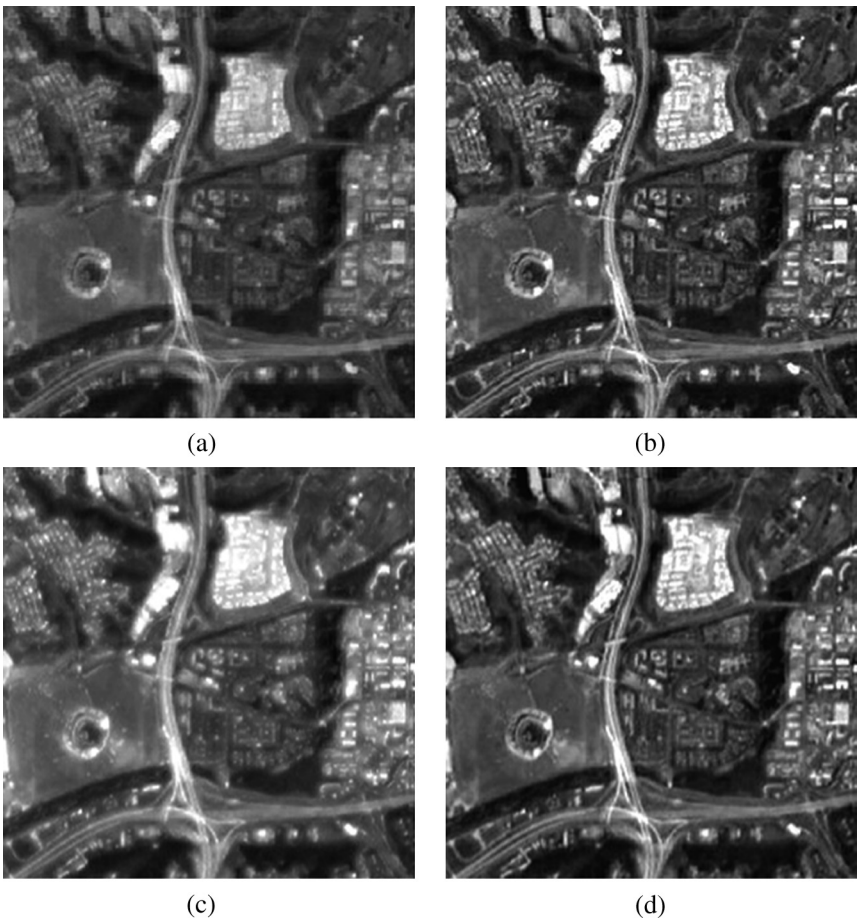

Fig. 10 The fused images of different algorithms: (a) principal component analysis (PCA), (b) Laplacian pyramid, (c) ratio pyramid, and (d) the proposed fusion algorithm.

Table 3 Statistics evaluation of different fusion methods.

Evaluation/ methods	PCA	Laplacian pyramid	Ratio pyramid	Bandelet
Standard deviation	42.0492	49.6877	50.2504	52.1755
Average gradient	5.7407	7.1023	6.9574	10.0934
Entropy	7.332	7.5029	7.5213	7.6567
RESE	0.0238	0.0222	0.0132	0.0174
SSIM	0.7791	0.8210	0.6272	0.8675

image means the similarity of the two images, where the maximum is one. The Bandelet transform fusion algorithm is the optimal one from the experiments above, especially, for the case that abundant texture features are contained in the original images.

4 Conclusion

We have presented a fusion algorithm between hyperspectral images and high-resolution images by using PCA and Bandelet transform. An original hyperspectral image is separated into every single component. Subsequently, Bandelet coefficients and geometry flows are calculated by using the second generation Bandelet transform. The data of Bandelet coefficients and geometry flows are then performed by PCA. The PC is replaced by the high-resolution image. The fused image is, finally, reconstructed by taking inverse PCA and Bandelet transform. Some numerical simulations have demonstrated the validity and superior performance of the proposed fusion algorithm.

Acknowledgments

This work was supported by the National Natural Science Foundation of China (Grant No. 11104049) and Specialized Research Fund for the Doctoral Program of Higher Education (Grant No. 20102302120009) and the Program for New Century Excellent Talents in University (NCET-12-0148). Thanks are due to Chengwei Yang for assistance with the experiment and Yatao Liu for valuable discussion. The authors are indebted to the reviewers for their helpful comments.

References

1. L. Guo, H. Li, and Y. Bao, *Image Fusion*, Electronic Industry Press, Beijing (2008).
2. B. Hou, W. Qiao, and Z. Sun, "Remote-sensing image fusion based on HIS transform and à trous wavelet decomposition," *J. Nanjing Norm. Univ. Nat. Sci.* **29**, 116–120 (2006).
3. J. Yan and X. Qu, *Analysis and Application Beyond Wavelet*, National Defence Industry Press, Beijing (2008).

4. G. Peyré and S. Mallat, "Discrete Bandelets with geometric orthogonal filters," in *IEEE Int. Conf. Image Process.*, Vancouver, pp. 65–68 (2005).
5. X. Qu et al., "A novel image fusion algorithm based on Bandelet transform," *Chin. Opt. Lett.* **5**(10), 569–572 (2007).
6. H. Chen and Y. Wang, "Research on image fusion algorithm based on Laplacian pyramid transform," *Laser Infrared* **39**, 439–442 (2009).
7. C. Chen and G. Hepner, "Fusion of hyperspectral and radar data using the IHS transformation to enhance urban surface features," *ISPRS* **58**(1–2), 19–30 (2003).
8. X. Ma and L. Peng, "PCA-based Laplacian pyramid in the image fusion," *Comput. Eng. Appl.* **42**, 211–213 (2010).
9. W. Yang and Y. Gong, "Multi-spectral and panchromatic images fusion based on PCA and fractional spline wavelet," *Int. J. Remote Sens.* **33** (22), 7060–7074 (2012).
10. W. Zhu and Q. Li, "Image fusion algorithm based on the second generation Bandelet," in *E-Product E-Service, and E-Entertainment (ICEEE)*, Henan, China, pp. 1–3 (2010).
11. W. Chang and L. Guo, "Hyperspectral image fusion based on PCA and contourlet transform," *J. Astronaut.* **30**, 2360–2365 (2009).
12. X. Li and J. Su, "Electron probe micro-area image fusion based on second generation Bandelet transform," in *Comput. Commun. Control Manage.*, Sanya, China, pp. 360–363 (2009).
13. H. Wang and L. Zhang, "Research on the application of image fusion and second-generation Bandelet transform in image denoising," in *Int. Conf. on Mechatronic Science, Electric Engineering and Computer (MEC)*, Jilin, China, pp. 1070–1073 (2011).
14. X. Qu and J. Yan, "A novel image fusion algorithm based on Bandelet transform," *Chin. Opt. Lett.* **5**(10), 569–572 (2007).
15. D. Donoho, "Wedgelets: nearly-minimax estimation of edges," *Ann. Stat.* **27**(3), 859–897 (1999).
16. Z. Hu and W. Gong, "Multi-resolution remote sensing image registration using differential evolution with adaptive strategy selection," *Opt. Eng.* **51**(10), 101707 (2012).
17. Q. Wang and Z. Wang, "Color image registration based on quaternion Fourier transformation," *Opt. Eng.* **51**(5), 057002 (2012).
18. W. Zhu and Q. Li, "Hyperspectral remote sensing images fusion algorithm based on second generation Bandelet and PCA transform," *J. Tongji Univ.* **39**, 1068–1073 (2011).
19. H. Lu and S. Nakashima, "An improved method for CT/MRI image fusion on Bandelets transform domain," *Appl. Mech. Mater.* **103**, 700–704 (2011).
20. H. Lu and Q. Wu, "Color image fusion based on PCA and wavelet frame transform," *Comput. Simul.* **24**, 202–205 (2007).
21. Q. Yang and K. Wang, "Fusion algorithm research based on the band compute and PCA transform," *Sci. Surv. Mapp.* **34**, 110–112 (2009).
22. J. Dou and J. Li, "Image fusion quality assessment based on discrete cosine transform and human visual system," *Opt. Eng.* **51**(9), 097002 (2012).

Xiaoping Du is a professor and supervisor of PhD candidates of Department of Space Command, Academy of Equipment, Beijing, China. She received the BEng and MEng degree in instrument science and technology from National University of Defense Technology, Hunan, China, in 1989, 1999, and the PhD degree from Beijing institute of technology, Beijing, China, in 2004. Her research interest covers hyperspectral image processing, target optical properties research and target detection.

Hang Chen received the BEng degree in photoelectric information engineering from Harbin Institute of Technology, Harbin, China, in 2011. He is a master's degree candidate in the Academy of Equipment, Beijing, China. His research interests include hyperspectral image processing, image recognition and image encryption.

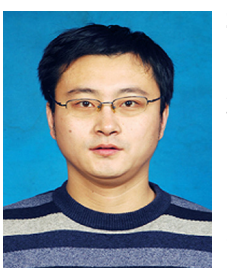

Zhengjun Liu received the BEng, MEng, and PhD degrees from Harbin Institute of Technology, Harbin, China, in 2002, 2004, and 2007, respectively. He is an associate professor Harbin Institute of Technology and a member of the optical society of America. He has published over 50 research papers in journals. His research interests include physical optics, optical information security algorithm and image processing.

Biographies and photographs of the other authors are not available.